*Clay Minerals* (2024), **59**, 100–112
doi:10.1180/clm.2024.9

CAMBRIDGE UNIVERSITY PRESS

**Article**

# Compressed earthen blocks using alluvial clays from Mbam: performance comparison using statistical analysis of cement *vs* heat-stabilized blocks

Christophe Enock Embom[1], Joël Fabrice Nyemb Bayamack[2], Arnaud Ngo'o Ze[1], Jacques Richard Mache[3], Jean Aimé Mbey[4]* and Vincent Laurent Onana[1,5]

[1]Department of Earth Sciences, Faculty of Science, University of Yaoundé I, PO Box 812, Yaoundé, Cameroon; [2]Department of Earth Sciences, Faculty of Science, University of Douala, BP: 24517 Douala, Cameroon; [3]Department of Mining Engineering, School of Mining Engineering, University of Ngaoundere, PO Box 115, Meiganga, Cameroon; [4]Department of Inorganic Chemistry, Faculty of Science, University of Yaoundé I, PO Box 812, Yaoundé, Cameroon and [5]Department of Geosciences and Environment, University of Ebolowa, PO Box 886, Ebolowa, Cameroon

**Abstract**

In the present study, a comparison of the thermal-insulation and mechanical performances of cement and heat-stabilized compressed earthen blocks (CEBs) was carried out to determine the factors which influence those properties. The raw clays used consist mainly of kaolinite, orthoclase and quartz. The mechanical strength increased with increase in both the amount of cement added and the firing temperature. However, the responses are better for cement-stabilized CEBs. The thermal insulation of fired bricks is greater than that of cement-stabilized bricks. This difference was related to the decrease in porosity and the formation of continuous-surface. The decrease in thermal insulation is mainly related to the formation of continuous-surface in cement-stabilized CEBs, whereas in the fired CEBs, it is due to the modification of pore volume. The mineralogy of the raw clays is statistically correlated to porosity and continuous-surface development that were confirmed as the main factors in the modification of both the mechanical strength and the thermal insulation. In cement-stabilization, the decrease in insulation is due to the development of continuous surface, while for heat-stabilization, mineral transformations during the sintering reduced continuous-surface formation and the insulation was controlled by both radiation and reduced surface conduction. The influence of the mineralogy of the raw material shows that clay content favours the insulation in fired bricks obtained at $T \leq 1000$°C, while sand contents favour densification. In contrast, clay contents reduce the mechanical response of cement-stabilized material due to limited cement–clay interactions. In general, the mechanical response is more favourable in cement stabilization, while thermal insulation is better in fired bricks.

**Keywords:** Kaolinite; mechanical strength; mineralogy; thermal insulation; statistical analysis

(Received 10 January 2024; revised 22 March 2024; Accepted Manuscript online: 24 April 2024; Associate Editor: Michele Dondi)

Providing people with affordable housing of good quality is a global challenge. This need justifies the extensive research in this field in both developing and developed countries (Taallah *et al.*, 2014). In the past, this sector relied on the use of natural materials, including earthen materials (Fabbri *et al.*, 2018; Elavarasan *et al.*, 2021) which were used because of their abundance and low cost and minimal energy requirement (Gallipoli *et al.*, 2017; Hadji *et al.*, 2020). The use of earthen materials often combines various construction techniques and standards. These include rammed earth, cob, stucco, adobe, CEBs and terracotta (Dos Santos *et al.*, 2014; Van Damme & Houben, 2018). Unfortunately, these construction products are all sensitive to water and show limited strength. As a result, their durability is poor (Elavarasan *et al.*, 2021; Benzerara *et al.*, 2021). The poor durability combined with poor mastery of building techniques, as well as disputes over procedures and standards for assessing earth construction performances, have led to the replacement of the earthen materials by industrial materials, such as concrete, steel, wood and synthetic materials (Fabbri *et al.*, 2018; Elavarasan *et al.*, 2021). However, wood construction has a large environmental impact through deforestation and concrete, steel and synthetic constructions are major causes of carbon emission (Giada *et al.*, 2019; Benzerara *et al.*, 2021; Belarbi *et al.*, 2022). In addition, construction using these industrial materials entails significant energy consumption (Giada *et al.*, 2019; Hadji *et al.*, 2020; Belarbi *et al.*, 2022). However, in the current context of sustainable development, energy supply is pivotal. Improvement is needed, especially in developing countries (Kaygusuz, 2012). Buildings that are sustainable, ecological and cost-effective bring focus to issues of material selection and processing. A return to the use of earth in the building industry is becoming a topic of interest for building improvement (Taallah

**Corresponding author:** Jean Aimé Mbey; Email: jean-aime.mbey@facsciences-uy1.cm
**Cite this article:** Enock Embom C, Nyemb Bayamack JF, Ngo'o Ze A, Mache JR, Mbey JA, Onana VL (2024). Compressed earthen blocks using alluvial clays from Mbam: performance comparison using statistical analysis of cement *vs* heat-stabilized blocks. *Clay Minerals* **59**, 100–112. https://doi.org/10.1180/clm.2024.9

*et al.*, 2014; Fabbri *et al.*, 2018; Okewale & Grobler, 2022). Earthen constructions provide much better comfort for residents through thermal insulation (Zhang *et al.*, 2017). The need to guarantee mechanical performance and consequently, durability, is crucial (Giada *et al.*, 2019; Benzerara *et al.*, 2021). Numerous studies have been carried out on improving the thermal and mechanical performances of earthen constructions. Earth-earth, earth-cement, earth-fly ash, earth-gypsum, earth-plant fibers and even earth-geopolymer mixtures increase the mechanical performances of the resulting bricks. Thermal performances remain similar to those of CEBs (Taallah *et al.*, 2014; Zhang *et al.*, 2017; Sore *et al.*, 2018; Van Damme & Houben, 2018; Elavarasan *et al.*, 2021; Hadji *et al.*, 2020; Belarbi *et al.*, 2022). In addition if additives to earthen block formulation improve their mechanical performance, this is achieved through heat treatment, which also affects the thermal performance (Bourret *et al.*, 2015; Debnath *et al.*, 2022). The intrinsic characteristics of each soil affect the performance irrespective of treatment. The present study aimed to compare the mechanical and thermal performances of cement- or heat-stabilized blocks using statistical analysis. The proposed comparison may help to identify the factors that affect the insulation behaviour and/or the mechanical response of the stabilized CEB and thus justify decisions about the type of stabilized CEB to be used with respect to the performance required or the environment in which the building is to be placed and its ultimate use. The physical and thermal parameters of specimens and their mechanical responses were evaluated. Statistical tools are used for a better understanding of the performance differences and the identification of the factors affecting the performance of the materials.

## Materials and analytical methods

### Materials

Five alluvial clayey samples named MN11, MN14, MN22, BP1 and BM2 were collected along the Mbam River bank in Central Africa. This area is located between 10°58'30"–11°20'30" East longitude and between 4°40'30"–5°01'15" North latitude. Approximately 70 kg of each sample was collected in polyethylene bags for laboratory testing. Portland cement, CEM II class 42.5 R (NF EN 197-1), was used to improve the mechanical performance of raw specimens. This is a commonly used hydraulic binder in building materials and is composed of ∼65% Portland clinker and ∼35% other constituents.

### Analytical methods

#### X-ray diffraction and X-ray fluorescence spectroscopy

The mineralogical and the major-element compositions of the materials studied were determined by X-ray diffraction (XRD) and X-ray fluorescence (XRF), respectively, at the University of Liège, Belgium. The XRD was performed with a Bruker D8 Advance Eco diffractometer, using Cu-*K*α radiation (λ = 1.5418 Å) at 40 kV and 30 mA. The powder XRD patterns were recorded over the range 2–70°2θ with a scanning step size of 1°2θ/min. The XRF analysis was conducted on fusion beads prepared at 1100°C, after diluting in lithium tetraborate flux at a 5:1 sample:flux ratio.

#### Semi-quantitative analysis

The mineralogical assemblage from non-oriented powder XRD was coupled to the chemical analysis of major elements for a semi-quantitative estimation of minerals present using Equation 1 proposed by Yvon *et al.* (1982).

$$T(x) = \sum_{1}^{n} Mi \times Pi(x) \quad (1)$$

where $T(x)$ = percentage of oxide of chemical element $x$; $Mi$ = percentage of mineral $i$ in the sample containing the chemical element $x$; $Pi(x)$ = proportion of element $x$oxide in mineral $i$ (calculated from the ideal mineral formula of the mineral being considered).

For the calculation, the following assumptions were adopted. The $Fe_2O_3$ was attributed to hematite or goethite; $K_2O$ was assigned to orthoclase and $TiO_2$ to rutile; $Al_2O_3$ was distributed in orthoclase and kaolinite; and the $SiO_2$ was distributed between orthoclase, kaolinite and quartz.

### Briquette preparation, physico-mechanical and thermal characterization

Mechanical tests for flexural ($\sigma_f$) and compressive ($\sigma_c$) strengths were performed on test briquettes with dimensions of 80 mm × 40 mm × 20 mm and 40 × 40 × 40 mm. For thermal tests, 100 mm × 100 mm × 20 mm briquettes were used. To process these briquettes, the raw clays were oven-dried at 105°C for 24 h, then ground manually with a porcelain mortar, and, finally, sieved over a 1 mm sieve. All the formulations were moistened with 8–18% water on a dry basis for convenient molding before being compressed using a SPECAC laboratory hydraulic press of 10 tons at a load of 1.27 MPa. In the case of clay/cement mix, the clay/cement ratios on a dry basis were 3, 6, 9, 12 and 15wt.%. For the fired samples, the compressed blocks were dried at ambient at temperatures of ∼27 ± 1°C for 7 days, then dried at 105°C before firing at 800°C, 900°C, 1000°C and 1100°C in an electric muffle furnace at a firing rate of 5°C/min. Samples were soaked for 2h at each maximum temperature before cooling to room temperature. For clay/cement mixtures, the specimens were cured at room temperature (27± 1°C) for 28 days.

The particle-size distribution of the raw clays was determined by sieving and sedimentation. Sieving was used for the coarse and fine sand fractions, over 200 µm and 80 µm sieve respectively. The Robinson's pipette method was used to assess the silt- and clay-sized fractions.

The dry ($\rho_d$) and bulk ($\rho$) densities of raw clays and test briquettes were determined in accordance with ASTM C373-88. The linear shrinkage ($LS$) was determined according to the ASTM C326-03 standard. Equation 2 was used for the $LS$ calculation.

$$LS(\%) = [(L_0 - L_1)/L_0] \times 100 \quad (2)$$

Where $L_0$ is the block length after compaction and $L_1$ is the length after firing or after room drying for 28 days.

The apparent porosity ($n$) and the water absorption ($WA$) were determined according to Equations 3 and 4, respectively (ASTM C373-88).

$$n(\%) = [(M_2 - M_1)/(M_2 - M')] \times 100 \quad (3)$$

$$WA(\%) = [(M_2 - M_1)/M_1] \times 100 \quad (4)$$

Where $M_1$ is the specimen dry mass (g), $M_2$ is the specimen mass (g) after 24 h of immersion in water and $M'$ is the mass of the specimen while suspended in water.

The flexural strength ($\sigma_f$) was measured in a three-point bending configuration (ASTM C674-77) on an Instron 5582 press in accordance with Equation 5.

$$\sigma_f = 3PL/2lh^2 \quad (5)$$

where $P$ = load (N) at the breaking strength; $L$ = distance (mm) between the two basal supports; $l$ = specimen width (mm); $h$ = specimen thickness (m).

The uniaxial compressive strength ($\sigma_c$) test was performed using an Instron servo-hydraulic press, with a capacity of 250 kN. The loading speed was 0.01 MPa/s.

The thermal and mechanical properties were determined on both cement-stabilized and fired specimens. The thermal effusivity ($E$ in $JK^{-1}m^{-2}s^{-1/2}$), the specific heat capacity ($\rho c$ in $JK^{-1}m^{-3}$), the diffusivity ($\alpha$ in $m^2s^{-1}$) and the conductivity ($\lambda$ in $Wm^{-1}K^{-1}$) were determined using the asymmetric hot plate method (Bal *et al.*, 2012, 2013). A material's thermal effusivity refers to its aptitude to exchange heat with its environment. The greater the value of $E$, the more the material absorbs energy from its environment (Yan & Song, 2021). $\alpha$ is a measure of the rate at which heat energy moves through the material, $\lambda$ refers to the material's capacity to allow a heat flow to pass through it and $\rho c$ is a property that measures the ability of a material to store heat energy. These measurements were carried out in a controlled room temperature (20 ± 1°C). The measurement principle involved the determination of $E$ and $\rho c$, assuming a unidirectional heat transfer at the center of the sample. $\alpha$ and $\lambda$ were deduced from $E$ and $\rho c$ according to Equations 6 and 7.

$$E = \sqrt{\lambda \rho c} \quad (6)$$

$$\alpha = \lambda / \rho c \quad (7)$$

### Statistical analysis

The statistical analysis was performed based on the results obtained from raw materials and on 50 individual samples, of which there were 30 cement-stabilized CEBs and 20 fired specimens. Nineteen variables were assessed. These variables included mineralogical components (quartz– Qz, kaolinite–Kln, hematite–Hem, goethite–Gth, illite–Iltand rutile–Rt), physical parameters (clay, silt, sand, ρ, $n$, $WA$ and $LS$), thermal parameters ($E$, α, λ and $\rho c$) and mechanical parameters ($\sigma_f$ and $\sigma_c$). The data was assembled in an Excel™ spreadsheet and then analyzed using the XLSTAT version 14.5.03 software. Correlation tests were carried out to assess relationships between the 19 quantitative variables considered in pairs. The summaries of these tests are represented below using correlation matrixes. Principal Component Analysis (PCA) was also carried out to assess possible relationships linking the 19 quantitative variables. Data from the 30 cement-stabilized CEBs and from the 20 fired specimens were grouped to obtain a single data set. The advantage of this statistical technique is that it synthesizes the information without truncating it. From an 'n'-dimensional space defined by a 'p' number of initial variables, the PCA determines a subspace of smaller dimension by searching for new variables (principal components). These new variables are often linearly independent but explain, at best, all the observations (De Lagarde, 1983). Agglomerative Hierarchical Clustering (AHC) (Ward, 1963) was executed to perform the PCA. The principle of this other technique is to construct natural groups such that specimens in the same group are similar and those in various groups are dissimilar (Bray & Curtis, 1957).

## Results and discussion

### Raw samples physical parameters and mineral and chemical compositions

The studied materials consisted of clay (29.38–55.88%), silt (15.67–27.27%) and sand (20.04–52.59%). In the ternary diagram soil classification (Davis & Bennett, 1927), the materials are classified as sandy heavy clays (MN14, MN22, BP1 and BM2) and sandy clays (MN11). Using the Winkler diagram of grain-size classification, the samples are suitable for brick manufacturing (Fadil-Djenabou *et al.*, 2015; Ndjigui *et al.*, 2021). The dry densities ($\rho_d$) are 1.58–1.74 g/cm$^3$ (Table 1), with an average of 1.68 g/cm$^3$. These values are consistent with the clayey nature of the raw materials.

The XRD traces of the raw clays are presented in Fig. 1. The clays consist of kaolinite, quartz and orthoclase (K-feldspar) as the main phases, associated with hematite/goethite, rutile and traces of anorthite and augite. The main chemical components are $SiO_2$(55.12–71.79%), $Al_2O_3$(13.68–20.58%) and $Fe_2O_3$(2.8–8.68%). Minor components are $TiO_2$(1.37–1.58%)$P_2O_5$(< 0.09%) and total fluxes (MnO, MgO, CaO, $Na_2O$ and $K_2O$)(2.61–4.36%, Table 1). The elemental composition is in accordance with the mineralogical composition from the XRD analysis. Coupling the chemical composition with the mineralogical assemblage, a semi-quantitative evaluation of the mineral composition was performed which led to the following mineral abundances:

**Table 1.** Physical parameters and mineralogical and chemical compositions of the raw materials.

| Parameters | MN11 | MN14 | MN22 | BP1 | BM2 |
|---|---|---|---|---|---|
| Clay | 29.38 | 55.88 | 39.31 | 38.06 | 52.69 |
| Silt | 18.03 | 20.83 | 15.67 | 26.83 | 27.27 |
| Sand | 52.59 | 23.29 | 45.02 | 35.11 | 20.04 |
| Sum | 100 | 100 | 100 | 100 | 100 |
| Dry density (g/cm$^3$) | 1.74 | 1.68 | 1.70 | 1.71 | 1.58 |
| Quartz | 48.3 | 27.0 | 44.2 | 30.1 | 29.3 |
| Kaolinite | 26.9 | 47.8 | 37.6 | 40.6 | 45.8 |
| Hematite | 2.8 | – | – | – | 6.8 |
| Goethite | – | 8.6 | 4.5 | 7.1 | – |
| Orthoclase | 16.7 | 9.1 | 8.5 | 15.4 | 11.0 |
| Rutile | 1.5 | 1.4 | 1.5 | 1.6 | 1.6 |
| Anorthite | ϵ | ϵ | ϵ | ϵ | ϵ |
| Augite | ϵ | – | ϵ | ϵ | ϵ |
| $SiO_2$ | 71.59 | 55.12 | 67.24 | 59.04 | 57.71 |
| $Al_2O_3$ | 13.68 | 20.58 | 16.43 | 18.9 | 20.13 |
| $Fe_2O_3$ | 2.8 | 8.68 | 4.53 | 7.15 | 6.83 |
| MnO | 0.03 | 0.04 | 0.02 | 0.03 | 0.06 |
| MgO | 0.29 | 0.71 | 0.33 | 0.82 | 1.01 |
| CaO | 0.55 | 0.44 | 0.52 | 0.51 | 0.63 |
| $Na_2O$ | 0.36 | 0.36 | 0.28 | 0.39 | 0.02 |
| $K_2O$ | 2.82 | 1.54 | 1.44 | 2.61 | 1.86 |
| $TiO_2$ | 1.5 | 1.37 | 1.48 | 1.58 | 1.57 |
| $P_2O_5$ | 0.05 | 0.04 | 0.04 | 0.05 | 0.08 |
| LOI | 5.61 | 11.58 | 7.67 | 8.74 | 10.43 |

ϵ = trace.

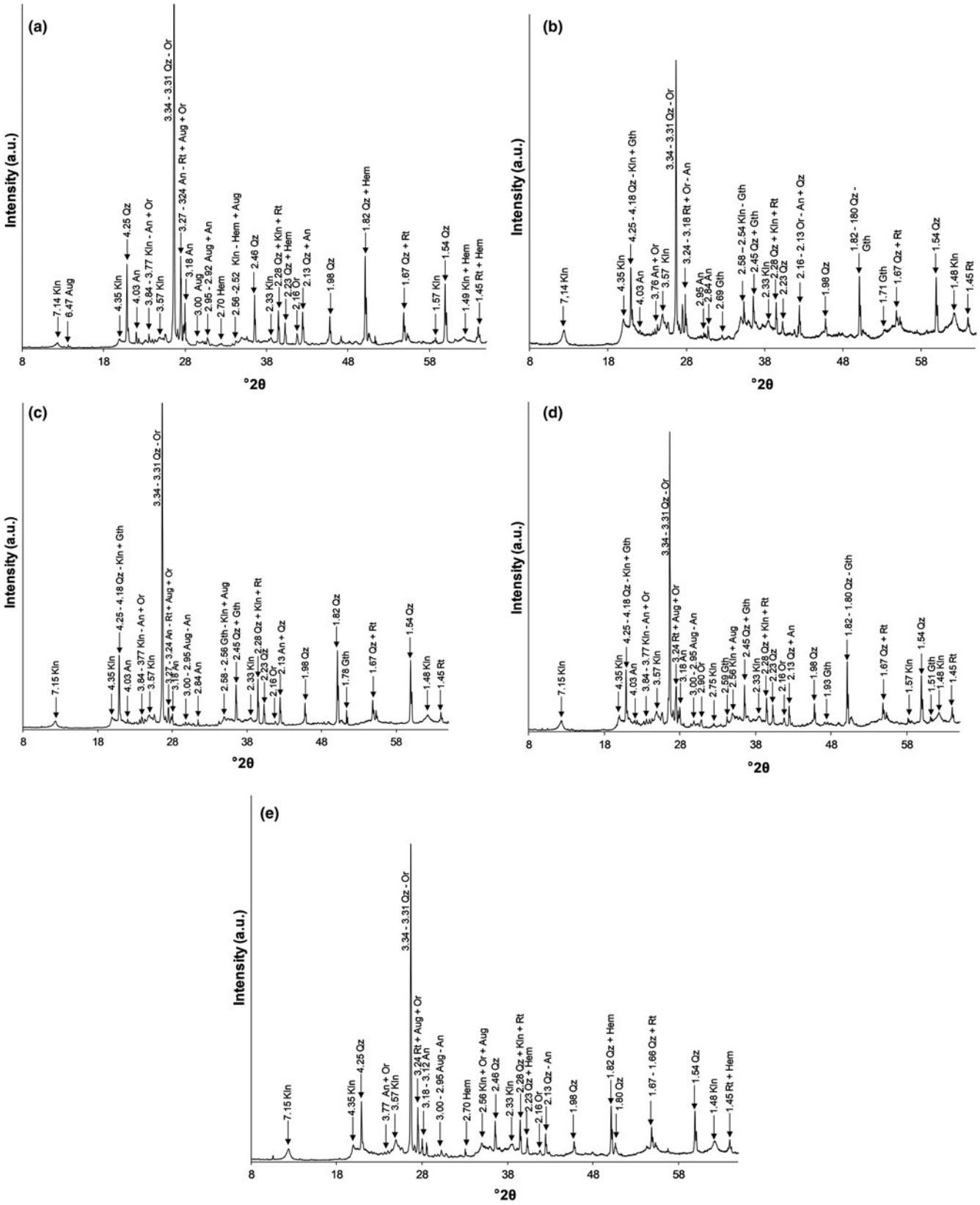


**Figure 1.** XRD patterns of raw materials: (a) MN11; (b) MN14; (c) MN22; (d) BP1 and (e) BM2. (The numbers indicate the *d* value, in Å, associated with the reflection.)

quartz 27.0–48.3%; kaolinite 26.9–47.8%; orthoclase 8.5–16.7%; hematite/goethite 2.8–8.6%; and rutile 1.4–1.6% (Table 1). The kaolinite contents for all the samples are of interest in terms of their use in construction and building materials. Due to the quartz contents, reduced swelling, shrinkage and cracking in wet or dry states are expected (Gallipoli *et al.*, 2017; Van

Damme & Houben, 2018). Orthoclase and flux contents, at suitable temperatures, favour the vitrification of the fired bodies from the clays.

### *Cement-stabilized specimens: physical, thermal and mechanical behaviours*

The bulk density of cement-stabilized specimens varies with the cement contents (Table 2), ranging between 2.00 and 2.29 g/cm$^3$, which are in the range of bulk densities for cement-stabilized CEB (1.6–2.2 g/cm$^3$) recommended by the International Center for Earthen Architecture (Nshimiyimana *et al.*, 2020). The addition of cement increases the density of all the samples. Although the clay compositions and processing are different, the density evolution observed here is similar to the behaviour of clays reported from Burkina Faso, using calcium carbide residues for stabilization (Nshimiyimana *et al.*, 2020). The calcium carbide, as Portland cement in hydrate mixes, leads to the formation of calcium silicate hydrate (C-S-H) which is the main cause of the observed trend. Optimal values are achieved at 9% (dry basis) for MN14 and BM2. Slightly higher values of densities for specimens made with MN11, MN22 and BP1 are related to quartz contents, which are greater for these samples. In general, the limit value for cement addition to improve density is related to the grain-size distribution and the mineralogy. In the present study, it is assumed that the changes in size distribution after addition of 9% cement are due to the replacement of a significant amount of larger particles, mainly associated with quartz, which have high density. At lower contents (<9%), the increase in density is guided by the integration of smaller cement particles within holes in the agglomerated particles of the clayey sample (Taallah *et al.*, 2014).

The linear shrinkage was not measurable, indicating insignificant shrinkage for these specimens. This trend can be associated with the presence of channels through which the excess fluid is drained with almost no displacement of the structural grains. The porosity ($n$) and water absorption ($WA$) in all specimens at 0% cement and in specimens based on MN14 and BM2 materials, stabilized at 3 and 6%, were not determined due to the collapse of the specimens after immersion in water. The destruction in water is linked to weak cohesion between the particles of these specimens. This is caused by the abundant clay fraction of these samples (Walker & Stace, 1997; Taallah *et al.*, 2014). In specimens in which structures were preserved, the values of $n$ ranged between 16.97 and 23.04%, while $WA$ ranged from 4.02 to 10.99% (Table 2). The $WA$ slightly increased for the MN14 and BM2 samples, while it decreased for the MN11, MN22 and BP1samples with greater cement contents. The porosity reduction in these specimens is linked to the progressive filling of pores by cement, which decreases the $WA$. Pore filling contributes to matrix reinforcement in specimen structures and to specimen densification (Taallah *et al.*, 2014; Zhang *et al.*, 2017; Sore *et al.*, 2018). Absorbed water is generally stored in pores. As the volume of pores decreases, so does the amount of water that can be absorbed. For MN14 and BM2, $n$ is almost stabilized as a result of addition of 9% cement. This is probably due to the increased cohesion brought on by larger cement particles that agglomerate the clay particles. However, the porosity of these samples (MN14 and BM2) remains higher in comparison to the remaining samples, due to a coarse agglomeration that develops a loose structure within the specimens. In general, a decrease in porosity

**Table 2.** Physical, thermal and mechanical characteristics of cement-stabilized specimens.

| Sample | Cement content (%) | ρ (g/cm$^3$) | $n$ (%) | $WA$ (%) | $E$ (J/K m$^2$ s$^{1/2}$) ×10$^3$ | α (m$^2$/s) ×10$^{-7}$ | λ (W/mK) ×10$^{-1}$ | ρc (J/K m$^3$) ×10$^6$ | $\sigma_f$ (Mpa) | $\sigma_c$ (Mpa) |
|---|---|---|---|---|---|---|---|---|---|---|
| MN11 | 0 | 2.04 | – | – | 1.23 | 4.90 | 8.62 | 1.76 | 0.77 | 1.53 |
| | 3 | 2.14 | 20.68 | 6.14 | 1.38 | 6.64 | 11.29 | 1.70 | 1.39 | 4.03 |
| | 6 | 2.16 | 19.35 | 5.29 | 1.50 | 8.16 | 13.52 | 1.66 | 2.68 | 12.70 |
| | 9 | 2.20 | 17.92 | 4.28 | 1.54 | 8.78 | 14.40 | 1.64 | 4.51 | 21.91 |
| | 12 | 2.23 | 17.23 | 4.18 | 1.56 | 9.98 | 15.54 | 1.56 | 4.66 | 23.40 |
| | 15 | 2.25 | 16.97 | 4.02 | 1.60 | 11.00 | 16.78 | 1.53 | 4.83 | 25.80 |
| MN14 | 0 | 2.00 | – | – | 1.20 | 2.93 | 6.48 | 2.21 | 1.35 | 2.77 |
| | 3 | 2.02 | – | – | 1.34 | 4.30 | 8.80 | 2.05 | 1.83 | 4.76 |
| | 6 | 2.09 | – | – | 1.36 | 5.24 | 9.81 | 1.87 | 2.92 | 10.17 |
| | 9 | 2.12 | 22.85 | 6.97 | 1.38 | 5.75 | 10.49 | 1.82 | 3.90 | 16.63 |
| | 12 | 2.10 | 22.91 | 8.01 | 1.32 | 5.23 | 9.55 | 1.83 | 4.12 | 17.22 |
| | 15 | 2.05 | 23.04 | 10.99 | 1.26 | 4.77 | 8.73 | 1.83 | 4.20 | 19.78 |
| MN22 | 0 | 2.07 | – | – | 1.15 | 3.83 | 7.09 | 1.85 | 0.85 | 1.89 |
| | 3 | 2.16 | 20.99 | 6.90 | 1.33 | 5.17 | 9.56 | 1.85 | 1.78 | 5.24 |
| | 6 | 2.19 | 19.91 | 5.04 | 1.40 | 6.34 | 11.14 | 1.76 | 3.27 | 14.79 |
| | 9 | 2.22 | 19.01 | 4.63 | 1.51 | 7.74 | 13.30 | 1.72 | 3.91 | 25.79 |
| | 12 | 2.25 | 18.44 | 4.39 | 1.54 | 8.15 | 13.94 | 1.71 | 4.63 | 27.71 |
| | 15 | 2.29 | 17.70 | 4.23 | 1.58 | 8.67 | 14.74 | 1.70 | 5.15 | 28.94 |
| BP1 | 0 | 2.09 | – | – | 1.22 | 3.50 | 7.22 | 2.07 | 0.87 | 1.98 |
| | 3 | 2.18 | 20.62 | 6.07 | 1.37 | 4.78 | 9.49 | 1.99 | 1.43 | 5.28 |
| | 6 | 2.20 | 19.74 | 5.77 | 1.49 | 6.57 | 12.05 | 1.83 | 2.76 | 12.82 |
| | 9 | 2.23 | 18.87 | 4.52 | 1.54 | 7.05 | 12.91 | 1.83 | 3.74 | 21.43 |
| | 12 | 2.24 | 18.49 | 4.43 | 1.53 | 7.05 | 12.88 | 1.83 | 4.17 | 24.34 |
| | 15 | 2.25 | 18.07 | 4.34 | 1.55 | 7.27 | 13.24 | 1.82 | 4.19 | 25.73 |
| BM2 | 0 | 2.01 | – | – | 1.17 | 2.98 | 6.38 | 2.14 | 1.30 | 2.36 |
| | 3 | 2.05 | – | – | 1.35 | 4.44 | 8.98 | 2.02 | 1.76 | 5.07 |
| | 6 | 2.08 | – | – | 1.47 | 5.41 | 10.83 | 2.00 | 3.05 | 9.18 |
| | 9 | 2.14 | 22.08 | 5.45 | 1.49 | 6.10 | 11.66 | 1.91 | 3.98 | 15.17 |
| | 12 | 2.10 | 22.53 | 7.21 | 1.34 | 4.89 | 9.38 | 1.92 | 4.01 | 17.91 |
| | 15 | 2.07 | 22.78 | 8.76 | 1.29 | 4.49 | 8.63 | 1.92 | 4.05 | 18.59 |

is registered while an increase in density is observed, which is in line with the observation by Zhang *et al.* (2017).

The thermal effusivity ($E$), diffusivity ($\alpha$) and conductivity ($\lambda$) of cement-stabilized CEB range from $1.15\times10^{3}$ to $1.60\times10^{3}$ $JK^{-1}m^{-2}s^{-1/2}$, $2.52\times10^{-7}$ to $1.10\times10^{-6}$ $m^{2}s^{-1}$ and $5.56\times10^{-1}$ to 1.68 $Wm^{-1}K^{-1}$ respectively. The values of these parameters are minimal in specimens without added cement (0%). They increase with addition of cement (Table 2) and are consistent with the increase in density (Bouguerra *et al.*, 1998; Sore *et al.*, 2018). These increases reduce the thermal insulation capability of cement-stabilized specimens. The latter have $E$ values comparable to those of laterite-stabilized products (Meukam *et al.*, 2004). Also, $\alpha$ and $\lambda$ increase with decreasing porosity (Table 2). The greater the $\lambda$ values, the more thermally conductive the material. The trends in the evolution of $\alpha$ and $\lambda$ in the studied materials are similar. Indeed, the largest values of $\alpha$ and $\lambda$ were recorded in cement-stabilized CEB, i.e. the densest, less porous CEB, where $E$ is large. It is then obvious that cement stabilization diminished the insulation capacity of the blocks (Belarbi *et al.*, 2022). This decrease is related to the difference between radiation and conduction within the block. In fact, radiation occurs in the air within the pores, and it is insulating (due to its low air conductivity, $\lambda_{air} \approx 0.026$ $Wm^{-1}K^{-1b}$) (Debnath *et al.*, 2022). Conduction occurs on a solid surface, with fewer insulating effects, given that the conductivity of a solid is greater than that of air (Sore *et al.*, 2018; Zhang *et al.*, 2017). Given that porosity is being reduced upon cement addition, the amount of trapped air (Sore *et al.*, 2018) and consequently, the radiation capability of the material are also reduced. The addition of cement favours solid surface development, which improves surface conduction.

The $\rho c$ value ranges from $1.53\times10^{6}$ to $2.21\times10^{6}$ $JK^{-1}m^{-3}$, leading to a heat mass capacity ($c$) range of $3440.2 \leq c \leq 4418.0$ $JK^{-1}kg^{-1}$, with the largest values in materials with 0% cement. Hence, cement stabilization reduces the heat-insulating capability of the blocks as $\rho c$ values decrease with increasing cement contents in all the specimens. However, these $\rho c$ values are relatively large compared to reported values of similar materials-based blocks from the literature (Meukam *et al.*, 2004; Mansour *et al.*, 2016; Sore *et al.*, 2018).

The flexural ($\sigma_f$) and compressive ($\sigma_c$) strengths range from 0.77 to 5.15 MPa and from 1.53 to 28.94 MPa, respectively (Table 2). The values of these parameters increase with increasing cement contents. This trend is in line with the development of more continuous solid surfaces, as suggested by the conductivity behaviour. The $\sigma_c$ values of cement-stabilized CEB, from 3% cement, are ≥4 MPa, which indicates that these blocks are suitable for construction of load-bearing walls in two-or three-storey buildings in dry environments (Reeves *et al.*, 2006; Murmu & Patel, 2018; Nshimiyimana *et al.*, 2020). In specimens with 0% cement, only MN14 and BM2-based specimens exhibit $\sigma_c \geq 2$ MPa, which makes them suitable for non-load-bearing structures in single-storey buildings in dry environments. The $\sigma_f$ and $\sigma_c$ values for MN14 and BM2 are the largest and are related to their clay contents, which are significant, compared to the remaining clayey materials. These clay mineral contents acted as a binding phase, which linked the coarse particles together in the CEB, ensuring the densification of the block (Van Damme & Houben, 2018). In cement-stabilized CEB, the cohesion between coarse particles is ensured by both the clay matrix and the cement. The hydration of cement particles leads to the formation of hydrated calcium silicate (C-S-H), which binds the coarse particles of the clayey materials, leading to a continuous surface that enhances the mechanical response (Sore *et al.*, 2018; John *et al.*, 2019). Clayey materials with moderate clay mineral contents (MN11, MN22 and BP1) exhibit a marked increase in mechanical response from the addition of 6% cement. The difference between samples having greater clay mineral contents (MN14 and BM2) is due to coarse particle content that interact with C-S-H to generate a denser structure.

### *Heat-stabilized specimens: mineralogical, physical, thermal and mechanical behaviour*

The mineralogical composition of fired samples is made up of quartz, hematite, orthoclase, rutile, anorthite and augite. A mullite diffraction peak at 3.40 Å is observed from 900°C (Fig. 2). Samples MN14 and BM2 fired at 1100°C also contain cristobalite (peaks at ~4.02 Å and ~2.48 Å). This mineralogy is consistent with that of raw materials due to the conversion of certain phases under thermal treatment. For instance, hematite forms from conversion of goethite at 250°C (Ruan *et al.*, 2001, 2002; Gialanella *et al.*, 2010). The disappearance of kaolinite is due to the conversion to metakaolinite at temperatures >600°C, which later leads to mullite crystallization and vitrification (Lee *et al.*, 2008; Wang *et al.*, 2017).

Linear shrinkage ($LS$) values are relatively low (1.11–7.22%) and increase with firing temperature (Table 3). Samples with large clay contents exhibit the largest values of $LS$. The small $LS$ values are consistent with the mineralogical assemblage of the raw materials, which are poor in fluxing agents, leading to limited formation of a vitreous phase. Hence, the main cause of $LS$ in these materials is capillary diffusion, which releases water molecules out of the structure during firing. The dehydration of oxyhydroxide minerals such as goethite and clay minerals are the main sources of $LS$ (He *et al.*, 2012). Hence, the largest values of $LS$in samples with large clay contents are explained. The $\rho$ values also increase with firing temperature, from 1.88 to 2.12 $g/cm^{3}$ (Table 3), due to densification, associated with the formation of denser phases such as mullite as from 900°C. These $\rho$ values are in line with the densities of kaolinite-based products reported in previous studies (Njeumen *et al.*, 2016; Pountouenchi *et al.*, 2023).

Porosity ($n$) and water adsorption ($WA$) decrease with increasing temperature. This trend is in accord with the fact that $WA$is linked to $n$. The $n$ decrease is associated with the enclosure of pores during sintering, resulting from vitreous phase formation. The values of $WA$ are small and they range from 4.12 to 7.21%. These low values indicate that all the materials are suitable for building materials and construction, according to Brazilian standard recommendations for $WA$ of <20% (Souza *et al.*, 2002; Onana *et al.*, 2019). Porosity ranges from 17.24 to 23.75% and is of interest for thermal isolation (Bories *et al.*, 2014). However, the firing temperature should not exceed1000°C in order to benefit from the pores in thermal insulation.

The thermal parameters of the fired bricks are reported in Table 3. All of the parameters decreased in the fired specimen at 800°C in comparison to the unfired blocks (sample dried under ambient conditions at ~28°C). The observed decrease of the parameters is related to kaolinite conversion into metakaolin upon dehydroxylation, which is a less conductive phase (Bourret *et al.*, 2015). Above 800°C, an increase in $E$, $\alpha$ and$\lambda$ is observed, resulting in a decrease in$\rho c$. The trend change after 800°C is associated with the crystallization and formation of phases such as mullite (Michot *et al.*, 2008) and the increase in structural

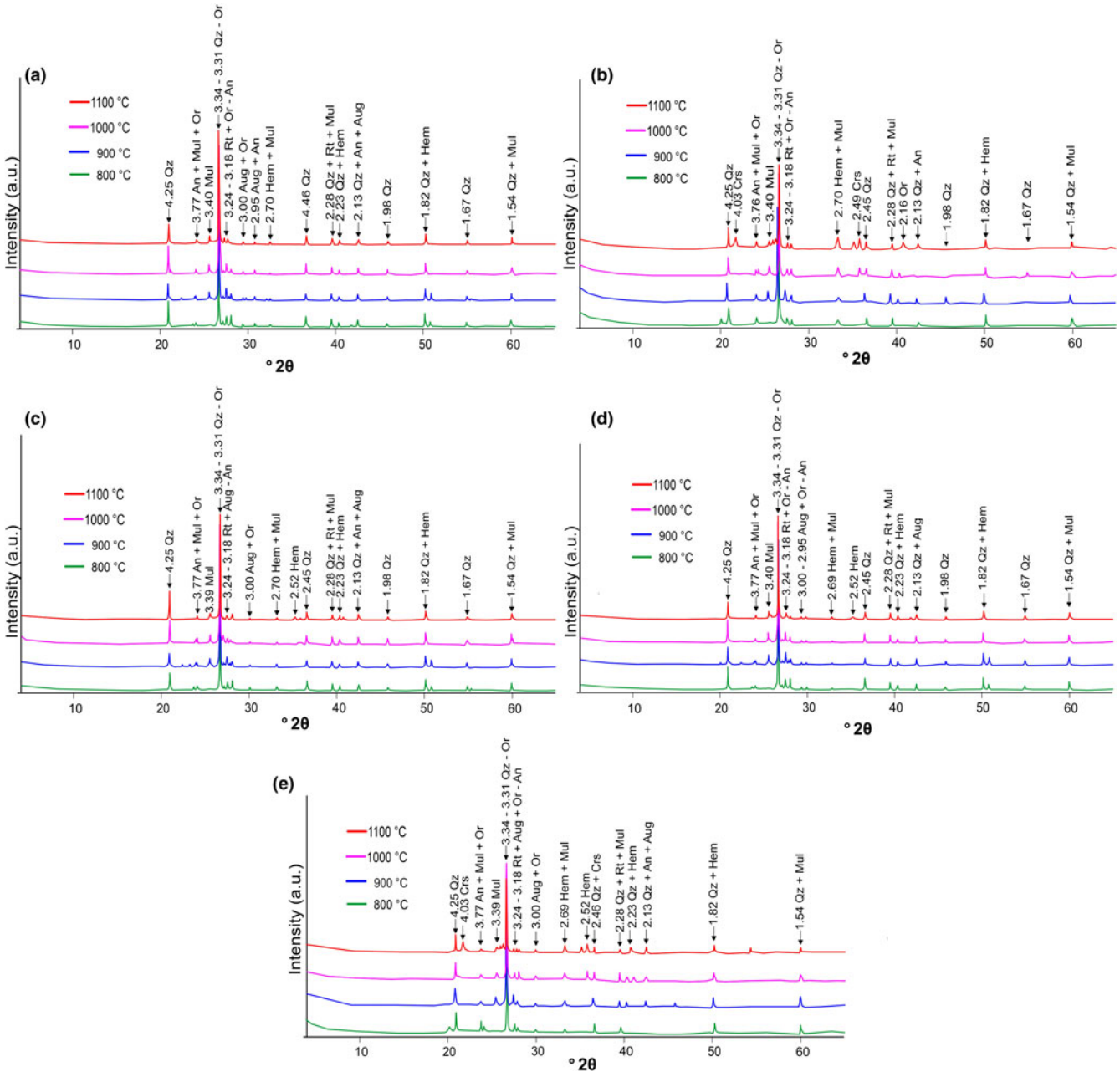


**Figure 2.** XRD patterns of fired briquettes: (a) MN11; (b) MN14; (c) MN22; (d) BP1 and (e) BM2. (The numbers indicate the *d* value, in Å, associated with the diffraction peak.)

organization of quartz, which is a highly conductive mineral in comparison to clay minerals (Yoon *et al.*, 2004). Hence, at low mullitization (<900°C), the most conductive blocks are made of samples rich in sand (quartz) fraction, namely MN11 and MN22. At temperatures >900°C, the degree of mullitization affects conductivity, with the clay-rich samples (MN14 and BM2) showing greater conductivity. The intermediate behaviour of sample BP1 is driven by its clay fraction (38.06%), which is in the same range as its sand fraction (35.11%). In addition, pore reduction upon firing contributes to increased conductivity due to increased surface conduction.

The ranges for $E$, $\alpha$ and $\lambda$ are $8.67\times10^{2}$ to $1.14\times10^{3}$ $JK^{-1}m^{-2}s^{-1/2}$, $2.22\times10^{-7}$ to $5.27\times10^{-7}$ $m^{2}s^{-1}$and $4.09\times10^{-1}$ to $8.24\times10^{-1}$ $Wm^{-1}K^{-1}$, while $\rho c$ values are in the range $1.55\times10^{6}$–$1.84\times10^{6}$ $JK^{-1}m^{-3}$ (Table 3). These values indicate that fired bricks are more heat insulating than cement-stabilized specimens.

The values of the flexural ($\sigma_f$) and compression ($\sigma_c$) strengths are listed in Table 3. They range from 1.63 MPa to 6.10 MPa and 5.71 MPa to 27.83 MPa, respectively. Both strengths increase with firing temperatures as reported in previous studies (Roudouane *et al.*, 2020; Onana *et al.*, 2019). These increases are obviously associated with increased densification during sintering. The firing promotes vitrification and the formation of denser phases such as mullite (Buchner *et al.*, 2021; Debnath *et al.*, 2022). The role of mullite on densification is further confirmed by the highest strengths registered for clay-rich samples, MN14 and BM2. According to the Brazilian standard reported by Souza *et al.* (2002), values of $\sigma_f \geq 2$ MPa and $\sigma_f \geq 5.5$ MPa are recommended

**Table 3.** Physical, thermal and mechanical characteristics of heat-stabilized specimens.

| Sample | Temperature (°C) | ρ (g/cm$^3$) | *n* (%) | *WA* (%) | *LS* (%) | *E* (J/K m$^2$ s$^{1/2}$) ×10$^2$ | α(m$^2$/s) ×10$^{-7}$ | λ (W/mK) ×10$^{-1}$ | ρ*c* (J/K m$^3$) ×10$^6$ | $\sigma_f$ (Mpa) | $\sigma_c$ (Mpa) |
|---|---|---|---|---|---|---|---|---|---|---|---|
| MN11 | 800 | 1.94 | 20.20 | 6.52 | 1.11 | 9.59 | 3.02 | 5.27 | 1.75 | 1.63 | 5.71 |
| | 900 | 1.95 | 20.06 | 6.18 | 1.50 | 9.71 | 3.51 | 5.75 | 1.64 | 1.66 | 6.82 |
| | 1000 | 1.99 | 20.01 | 5.69 | 1.71 | 9.86 | 3.86 | 6.12 | 1.59 | 1.73 | 6.98 |
| | 1100 | 2.03 | 19.98 | 5.42 | 1.80 | 10.76 | 4.83 | 7.48 | 1.55 | 1.84 | 7.80 |
| MN14 | 800 | 1.88 | 23.75 | 6.24 | 1.37 | 8.67 | 2.22 | 4.09 | 1.84 | 2.92 | 11.21 |
| | 900 | 1.96 | 21.81 | 6.01 | 2.24 | 9.11 | 2.49 | 4.54 | 1.83 | 4.15 | 17.81 |
| | 1000 | 2.02 | 19.55 | 5.66 | 3.74 | 11.06 | 4.33 | 7.28 | 1.68 | 4.88 | 24.83 |
| | 1100 | 2.12 | 17.24 | 4.12 | 7.22 | 11.35 | 5.27 | 8.24 | 1.56 | 6.10 | 27.83 |
| MN22 | 800 | 1.97 | 21.39 | 6.43 | 1.30 | 9.82 | 3.05 | 5.43 | 1.78 | 1.74 | 7.65 |
| | 900 | 2.03 | 20.89 | 6.06 | 1.64 | 10.31 | 3.64 | 6.22 | 1.71 | 1.88 | 7.97 |
| | 1000 | 2.07 | 20.48 | 5.88 | 1.84 | 10.62 | 4.17 | 6.86 | 1.65 | 2.09 | 8.79 |
| | 1100 | 2.10 | 19.57 | 5.63 | 2.25 | 10.81 | 4.47 | 7.23 | 1.62 | 2.69 | 10.44 |
| BP1 | 800 | 1.91 | 21.84 | 6.07 | 1.20 | 9.23 | 2.90 | 4.97 | 1.72 | 1.65 | 6.75 |
| | 900 | 1.93 | 20.57 | 5.92 | 1.52 | 9.43 | 3.05 | 5.21 | 1.71 | 1.75 | 7.44 |
| | 1000 | 1.99 | 19.65 | 5.79 | 1.78 | 10.41 | 3.87 | 6.47 | 1.67 | 1.92 | 7.85 |
| | 1100 | 2.02 | 19.32 | 4.97 | 1.93 | 10.55 | 4.31 | 6.93 | 1.61 | 2.36 | 8.90 |
| BM2 | 800 | 1.87 | 22.30 | 7.21 | 1.35 | 9.19 | 2.56 | 4.65 | 1.82 | 2.64 | 11.07 |
| | 900 | 1.93 | 21.37 | 6.27 | 2.05 | 9.64 | 2.94 | 5.23 | 1.78 | 4.31 | 16.34 |
| | 1000 | 1.96 | 19.95 | 6.14 | 3.63 | 1097 | 4.06 | 6.99 | 1.72 | 5.66 | 21.34 |
| | 1100 | 2.05 | 17.72 | 4.58 | 5.35 | 11.39 | 4.76 | 7.86 | 1.65 | 5.73 | 24.32 |

for structural brick making. Among the studied samples, MN14 and BM2 are suitable after firing at 800°C, while temperatures of at least 1000°C may be necessary for the other samples unless an amendment is made to reduce the firing temperatures.

### *Cement and heat-stabilized specimens: performance comparison using statistical analysis*

Comparison of average values of physical parameters shows that ρ is greater in cement-stabilized CEB than in fired bricks (Table 4), whereas *n* is greater in fired bricks than in cement-stabilized CEB. These two parameters affected both the thermal and mechanical behaviours of the specimens. Indeed, *E*, α and λ are smaller in fired bricks than in cement-stabilized CEB, indicating a greater thermal insulation capacity for fired bricks. In addition, the mechanical parameters $\sigma_f$ and $\sigma_c$ are greater in cement-stabilized CEB than in fired bricks. The comparison of standard deviation (SD) values (Table 4) shows that the thermal properties (*E*, α, λ and ρ*c*) and the compressive strength ($\sigma_c$) of the studied materials are more dispersed when stabilized with cement, while the flexural strength ($\sigma_f$) dispersion is greater for fired products. These differences in dispersion indicate that the changes in properties are more marked for cement stabilization than for heat stabilization; there is an optimal temperature beyond which the changes are less sensitive.

Tables 5 and 6 highlight the levels of correlation between physical, mineralogical, thermal and mechanical parameters. ρ is moderately negatively correlated with *n* in both cement-stabilized and heat-stabilized materials. These negative correlations agree with the *n* reduction upon either firing temperature increase or cement percent increase, confirming the results from the measured *n* (see previous sections). However, the level of correlation between ρ and *n* is greater (absolute value) in fired materials (R = –0.783) compared to cement-stabilized materials (R = –0.612), suggesting a possible additional factor on vitrification that is taking place in the firing process. As *LS* correlates positively with ρ (R = 0.592) and negatively with *n* (R = –0.731) in fired specimens, the *LS* should be considered to be the additional factor. The latter affects not only the total volume of the specimen, but also the volume of voids in the specimen, resulting in the improvement of the density along with vitrification.

ρ is strongly positively correlated with *E*, α and λ ($R \geq 0.840$) and negatively correlated with ρ*c* ($R \leq -0.717$). These trends indicate reduced insulation capacities of specimens with increasing densities and this is further confirmed by the fact that *n*, in contrast to ρ in the same specimens, is negatively correlated with *E*, α and λ ($R \leq -0.591$) and positively with ρ*c* ($R \geq 0.434$). Most of these correlations are high and linear (supplementary data Fig. S1a to S1i). Some of the correlations are average in cement-stabilized specimens when compared to heat-stabilized specimens, resulting in the fact that specimens are more insulating

**Table 4.** Statistical summaries of measured variables in cement and heat stabilized CEB.

| Stabilization | Statistics | ρ | *n* | *WA* | *LS* | *E*×10$^3$ | α×10$^{-7}$ | λ×10$^{-1}$ | ρ*c*×10$^6$ | $\sigma_f$ | $\sigma_c$ |
|---|---|---|---|---|---|---|---|---|---|---|---|
| Cement | Minimum | 2 | 16.97 | 4.02 | 0 | 1.15 | 2.93 | 6.38 | 1.53 | 0.77 | 1.53 |
| | Maximum | 2.29 | 23.04 | 10.99 | 0 | 1.60 | 11.0 | 16.8 | 2.21 | 5.15 | 28.94 |
| | Average | 2.14 | 20.01 | 5.79 | 0 | 1.40 | 6.07 | 10.9 | 1.84 | 3.07 | 14.16 |
| | SD | 0.08 | 1.7 | 1.51 | 0 | 0.13 | 2.01 | 2.76 | 0.16 | 1.39 | 9.09 |
| Firing | Minimum | 1.87 | 17.24 | 4.12 | 1.11 | 0.87 | 2.22 | 4.09 | 1.55 | 1.63 | 5.71 |
| | Maximum | 2.12 | 23.75 | 7.21 | 7.22 | 1.14 | 5.27 | 8.24 | 1.84 | 6.1 | 27.83 |
| | Average | 1.99 | 20.38 | 5.84 | 2.33 | 1.01 | 3.67 | 6.14 | 1.69 | 2.97 | 12.39 |
| | SD | 0.07 | 1.49 | 0.69 | 1.55 | 0.08 | 0.86 | 1.19 | 0.087 | 1.56 | 7.02 |

SD = standard deviation.

**Table 5.** Correlation matrix of variables in cement-stabilized CEB.

| Variables | Clay | Silt | Sand | Qz | Kln | Hem | Gth | Or | Rt | ρ | *n* | *WA* | *LS* | *E* | α | λ | Pc | σf | σc |
|---|---|---|---|---|---|---|---|---|---|---|---|---|---|---|---|---|---|---|---|
| Clay | **1** | | | | | | | | | | | | | | | | | | |
| Silt | **0.393** | **1** | | | | | | | | | | | | | | | | | |
| Sand | **−0.939** | **−0.685** | **1** | | | | | | | | | | | | | | | | |
| Qz | **−0.818** | **−0.763** | **0.933** | **1** | | | | | | | | | | | | | | | |
| Kln | **0.940** | **0.533** | **−0.944** | **−0.916** | **1** | | | | | | | | | | | | | | |
| Hem | 0.208 | **0.442** | −0.330 | −0.080 | 0.054 | **1** | | | | | | | | | | | | | |
| Gth | 0.332 | 0.015 | −0.269 | **−0.504** | **0.504** | **−0.817** | **1** | | | | | | | | | | | | |
| Or | **−0.707** | 0.236 | **0.471** | 0.292 | **−0.647** | 0.107 | −0.326 | **1** | | | | | | | | | | | |
| Rt | −0.356 | **0.580** | 0.065 | 0.029 | −0.185 | **0.473** | **−0.484** | **0.511** | **1** | | | | | | | | | | |
| ρ | **−0.630** | −0.233 | **0.586** | **0.456** | **−0.492** | −0.328 | −0.010 | 0.330 | 0.291 | **1** | | | | | | | | | |
| *n* | **0.665** | 0.277 | **−0.630** | **−0.535** | **0.599** | 0.210 | 0.154 | **−0.425** | −0.235 | **−0.612** | **1** | | | | | | | | |
| *WA* | **0.575** | 0.177 | **−0.522** | **−0.453** | **0.498** | 0.113 | 0.190 | −0.359 | −0.319 | **−0.598** | **0.873** | **1** | | | | | | | |
| *LS* | | | | | | | | | | | | | | | | | | | |
| *E* | **−0.444** | −0.096 | **0.388** | 0.319 | **−0.388** | −0.079 | −0.140 | 0.338 | 0.242 | **0.875** | **−0.591** | **−0.601** | | **1** | | | | | |
| A | **−0.641** | **−0.392** | **0.654** | **0.617** | **−0.664** | −0.119 | −0.268 | **0.408** | 0.094 | **0.856** | **−0.653** | **−0.571** | | **0.896** | **1** | | | | |
| Λ | **−0.587** | −0.294 | **0.575** | **0.524** | **−0.579** | −0.113 | −0.223 | **0.390** | 0.153 | **0.889** | **−0.648** | **−0.598** | | **0.956** | **0.986** | **1** | | | |
| ρc | **0.688** | **0.595** | **−0.768** | **−0.756** | **0.756** | 0.188 | 0.277 | −0.348 | 0.059 | **−0.717** | **0.434** | 0.324 | | **−0.654** | **−0.885** | **−0.825** | **1** | | |
| $\sigma_f$ | −0.019 | −0.087 | 0.048 | 0.070 | −0.038 | −0.006 | −0.029 | −0.043 | −0.041 | **0.637** | −0.187 | −0.125 | | **0.732** | **0.702** | **0.732** | **−0.572** | **1** | |
| $\sigma_c$ | −0.190 | −0.145 | 0.205 | 0.176 | −0.153 | −0.142 | 0.017 | 0.037 | 0.038 | **0.760** | −0.342 | −0.255 | | **0.777** | **0.761** | **0.790** | **−0.629** | **0.957** | **1** |

Values in bold are different from 0 with a level of significance, alpha = 0.05.

when heat-stabilized than when cement-stabilized. The correlation of these properties to the mineralogy of cement-stabilized specimens shows that quartz and kaolinite contents are the main sources of densification. Because quartz is denser than kaolinite, it is positively correlated with ρ(R = 0.456), whereas kaolinite is negatively correlated (R = –0.492). The negative correlation with kaolinite is probably associated with the poor interaction between the clay and the fine cement particles, which may not favour densification. In contrast, interactions with coarser quartz particles increase the densification. Correlations of the density with raw-sample mineralogy in fired specimens are not meaningful, as the changes in mineral forms of clays to mullite or of quartz to its polymorphs (such as cristobalite) should be considered. The same applies to the thermal parameters (Table 6). It is then postulated that the less insulating behaviour of the cement-stabilized CEB is due to pore organization defaults that favor surface conduction, in contrast to heat-stabilized specimens, in which the mineralogical conversion of the clay minerals and vitrification generate control of the pore structures, in which radiation in the trapped air is developed. However, the mechanical responses of the fired specimens are favorably correlated to kaolinite contents (R ≥ 0.695), as a result of their conversion during sintering in more dense phases such as mullite. The *LS* and the clay fraction, in heat stabilization, are positively linearly correlated with mechanical strength (supplementary data Fig. S1k to S1n). This is not the case in cement-stabilized CEB as there is almost no shrinkage.

Correlations between thermal (*E*, α and λ) and mechanical parameters ($\sigma_f$ and $\sigma_c$) are positive and significant (R ≥ 0.702) in cement-stabilized materials (Table 5), whereas for heat-stabilized materials, correlations are positive but less significant (R ≤ 0.526) (Table 6). The structure of the specimens is probably the main cause of the differences. In cement-stabilized materials, the formation of calcium silicate hydrate (C-S-H) favours the formation of continuous surface which improve mechanical responses but reduce insulation capacity as the surface conduction improves. In fired products, the sintering process implies the formation of a vitreous phase in which unmodified mineral grains are embedded together with the partial mineral conversion of some phases. This leads to less continuous surfaces that contribute to enhancement of insulation due to the reduction of surface conduction.

In the PCA, the cumulated percentage of variance (56.79) presented by the two axes F1 and F2 is not sufficient. To avoid misinterpretation of the graphic, the F1–F3 factorial plan has been added, for a cumulated percentage of variance of 71.09 (supplementary data, Table S1). Results relative to the contribution of variables for the construction of these axes show that thirteen parameters are well expressed. This contribution is supported by the square cosine method (supplementary data Table S2). According to this method, clay, sand, Qz, Kln, ρ, *n*, α and λ on the F1 axis, $\sigma_f$ and $\sigma_c$ on the F2 axis, and silt, Hem, and Rt on the F3 axis are well represented. An interpretation based on *WA*, *E*, Gth and Or is to be considered secondary.

In the F1–F2 correlation circle (Fig. 3a), Kln and clay are positively correlated. These two variables are negatively correlated with Qz and sand. *E*, α, λ, ρ, $\sigma_f$ and $\sigma_c$ are close, i.e. positively correlated. These correlations corroborate observations made previously, i.e. the greater the value of ρ, the greater is *E*, α, λ, $\sigma_f$ and $\sigma_c$. In the F1–F3 factorial plan (Fig. 3b), sand and Qz are close to ρ, α and λ. This group of parameters is significantly negatively correlated with clay, Kln and *n*. These correlations reaffirm the impact of the mineralogical variation on the density and, consequently, on the thermal performance. The resulting clouds of individuals (Fig. 3c,d) show that the F1 axis almost separates cement-stabilized CEB from heat-stabilized specimens. This highlights the effect of the two stabilization techniques on the initial materials. The two groups can, however, be redistributed into three classes. Indeed, AHC organizes the cement and heat-stabilized materials studied into classes 1, 2 and 3 (Fig. 4). Class 1 groups both cement- (10 samples) and heat- (17 samples) stabilized CEB. This class is governed by moderate to large clay, sand, quartz and kaolinite contents (clay = 38.16%, sand = 41.97%, Qz = 40.71% and Kln = 35.75%) (supplementary data Table S3). Specimens in this class show good mechanical performances when cement-stabilized. In addition, they show good insulation capabilities and moderate to good mechanical performances when heat-stabilized. Class 2 (7 samples) consists only of cement-stabilized CEB and the controlling factors here are large clay and kaolinite, and moderate sand and quartz contents (clay = 49.42%, Kln = 44.92%, sand = 25.27% and Qz = 28.88%). Specimens in this class are marked by large insulation capacities and poor mechanical performances.

**Table 6.** Correlation matrix of variables in heat-stabilized specimens.

| Variables | Clay | Silt | Sand | Qz | Kln | Hem | Gth | Or | Rt | ρ | *n* | *WA* | *LS* | *E* | α | λ | ρc | $\sigma_f$ | $\sigma_c$ |
|---|---|---|---|---|---|---|---|---|---|---|---|---|---|---|---|---|---|---|---|
| Clay | **1** | | | | | | | | | | | | | | | | | | |
| Silt | 0.393 | **1** | | | | | | | | | | | | | | | | | |
| Sand | **–0.939** | **–0.685** | **1** | | | | | | | | | | | | | | | | |
| Qz | **–0.759** | –0.341 | **0.729** | **1** | | | | | | | | | | | | | | | |
| Kln | **0.940** | **0.533** | **–0.944** | **–0.903** | **1** | | | | | | | | | | | | | | |
| Hem | 0.208 | 0.442 | –0.330 | 0.190 | 0.054 | **1** | | | | | | | | | | | | | |
| Gth | 0.332 | 0.015 | –0.269 | **–0.609** | **0.504** | **–0.817** | **1** | | | | | | | | | | | | |
| Or | **–0.707** | 0.236 | **0.471** | **0.745** | **–0.647** | 0.107 | –0.326 | **1** | | | | | | | | | | | |
| Rt | –0.356 | **0.580** | 0.065 | 0.124 | –0.185 | **0.473** | **–0.484** | **0.511** | **1** | | | | | | | | | | |
| ρ | –0.063 | –0.397 | 0.198 | –0.071 | –0.073 | –0.282 | 0.139 | –0.261 | –0.252 | **1** | | | | | | | | | |
| *n* | 0.084 | –0.020 | –0.059 | –0.117 | 0.094 | –0.063 | 0.093 | –0.119 | –0.067 | **–0.783** | **1** | | | | | | | | |
| *WA* | –0.110 | –0.045 | 0.104 | 0.105 | –0.135 | 0.196 | –0.271 | 0.019 | 0.171 | **–0.778** | **0.805** | **1** | | | | | | | |
| *LS* | **0.550** | 0.165 | **–0.498** | –0.314 | **0.468** | 0.149 | 0.137 | –0.352 | –0.288 | **0.597** | **–0.731** | **–0.764** | **1** | | | | | | |
| E | 0.072 | –0.065 | –0.032 | –0.092 | 0.052 | 0.074 | –0.073 | –0.178 | –0.001 | **0.840** | **–0.868** | **–0.717** | **0.706** | **1** | | | | | |
| α | –0.092 | –0.134 | 0.123 | 0.081 | –0.112 | –0.018 | –0.063 | –0.004 | –0.026 | **0.881** | **–0.892** | **–0.807** | **0.665** | **0.951** | **1** | | | | |
| λ | –0.017 | –0.103 | 0.052 | 0.005 | –0.038 | 0.020 | –0.063 | –0.080 | –0.020 | **0.874** | **–0.893** | **–0.783** | **0.697** | **0.983** | **0.992** | **1** | | | |
| $\rho_c$ | **0.453** | 0.213 | –0.438 | –0.384 | 0.441 | 0.143 | 0.106 | –0.343 | –0.074 | **–0.760** | **0.783** | **0.723** | –0.382 | **–0.714** | **–0.883** | **–0.822** | **1** | | |
| $\sigma_f$ | **0.817** | 0.343 | **–0.775** | **–0.470** | **0.701** | 0.370 | 0.074 | **–0.500** | –0.270 | 0.284 | –0.420 | **–0.469** | **0.861** | **0.496** | 0.362 | 0.428 | 0.007 | **1** | |
| $\sigma_c$ | **0.810** | 0.280 | **–0.746** | **–0.473** | **0.695** | 0.268 | 0.161 | **–0.516** | –0.361 | 0.336 | **–0.455** | **–0.506** | **0.890** | **0.526** | 0.401 | **0.464** | –0.038 | **0.981** | **1** |

Values shown in bold are different from 0 with a level of significance, alpha = 0.05.

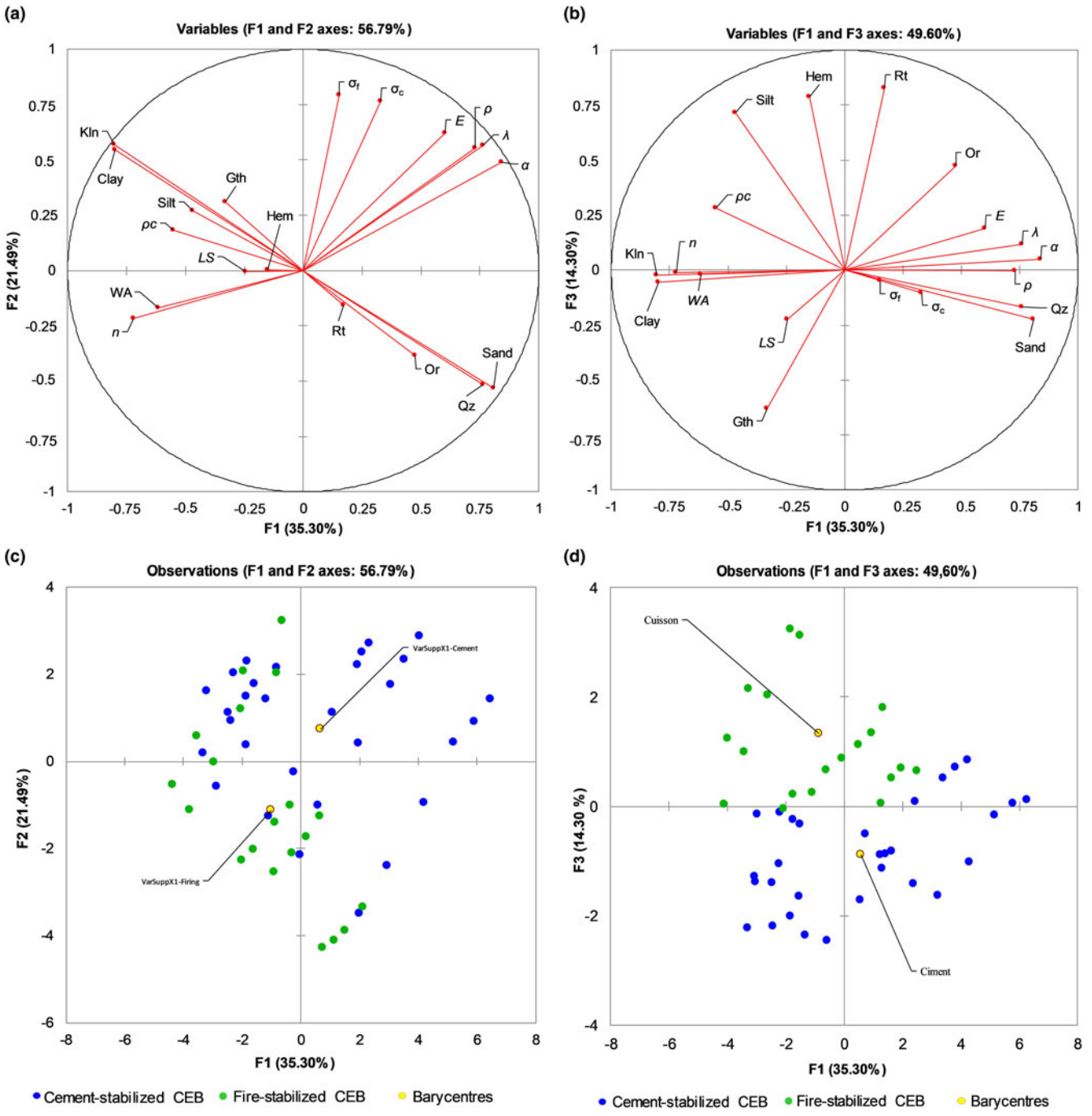


**Figure 3.** PCA of variables (a & b) and of individuals cements and heat stabilized CEB (c & d).

Similar to class 1, class 3 also consists of both cement- (13 samples) and heat- (3 samples) stabilized CEB. Here the governing factors are large clay and kaolinite, and moderate sand and quartz contents (clay = 48.56%, Kln = 44.26%, sand = 28.15% and Qz = 30.51%). Specimens in this class show moderate to high insulation capacities and moderate mechanical performances regardless of the stabilization type.

## Summary and conclusions

Clayey materials from the Mbam River banks were characterized and used in the manufacture of earthen building blocks. The aim was to evaluate their thermal and mechanical performances after cement- and heat-stabilization. These materials consist mainly of kaolinite, orthoclase and quartz with minor hematite, goethite, rutile, anorthite and augite. Their densities are consistent with their nature as soil materials, with variations associated with differences in mineral-phase contents, mainly kaolinite and quartz. Overall, the thermal insulation of the materials studied is satisfactory, with better performances for heat-stabilized specimens, especially those fired at temperatures of <1000°C. The insulation capacity of heat-stabilized specimens decreases with temperature increase as a result of pore reduction. However, the poor development of continuous surfaces allows the thermal insulation to remain

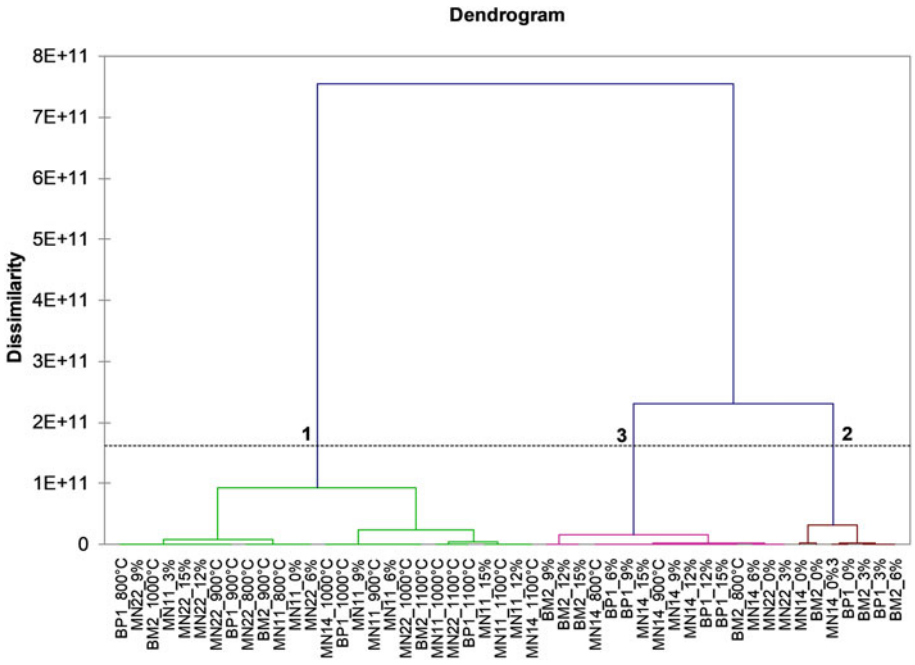


**Figure 4.** Dendrogram of cement and heat stabilized materials.

greater when compared to cement-stabilized specimens. The cement-stabilizedspecimens show greater mechanical responses than heat-stabilized specimens. Addition of ~9% cement is the ideal level for cement-stabilized specimens, particularly for those rich in kaolinite. Regarding the firing temperature, a minimum of 900°C should be recommended to obtain suitable fired bricks. It was established using statistics that the mineralogy of raw samples determines the insulation behaviour of the stabilized CEB. For fired samples, large clay contents favour insulation behaviour through the transformation of clay minerals during firing. Discontinuities arising from conversion of clay minerals and the formation of a vitreous phase cause reduced conduction surfaces, which enhance the thermal insulating performance. *LS* is an additional factor for porosity changes in heat stabilization. For cement-stabilized materials, the role of C-S-H in continuous surface development was proposed as a main cause of thermal insulation reduction. A large clay content does not favour the mechanical response in cement stabilization, due to poor clay–cement interaction. Coarse particles, such as sand, are needed to ensure good cohesion and interaction between the C-S-H and the fine fraction due to clay.

Overall, although the mineralogy of the starting material should be considered in relation to the performance needed, the mechanical responses are of more interest with cement stabilization, while thermal insulation is better using firing.

**Supplementary material.** To view supplementary material for this article, please visit https://doi.org/10.1180/clm.2024.9.

**Acknowledgements.** The Cameroonian Ministry of Higher Education is acknowledged for providing a research allowance for the modernization of university research to the teachers-researchers of state universities.

**Financial support.** This research did not receive any specific grant from funding agencies in the public, commercial, or not-for-profit sectors.

**Conflicts of interest.** The authors declare that they have no known competing financial interests or personal relationships that could have appeared to influence the work reported in this paper.

## References

Bal H., Jannot Y., Quenette N., Chenu A. & Gaye S. (2012) Water content dependence of the porosity, density and thermal capacity of laterite based bricks with millet waste additive. *Construction and Building Materials*, **31**, 144–150.

Bal H., Jannot Y., Gaye S. & Demeurie F. (2013) Measurement and modelisation of the thermal conductivity of a wet composite porous medium: Laterite based bricks with millet waste additive. *Construction and Building Materials*, **41**, 586–593.

Belarbi Y.E., Sawadogo M., Poullain P., Issaadi N., Hamami A.E.A., Bonnet S. & Belarbi R. (2022) Experimental Characterization of Raw Earth Properties for Modeling Their Hygrothermal Behavior. *Buildings*, **12**, 648. https://doi.org/10.3390/buildings12050648

Benzerara M., Guihéneuf S., Belouettar R. & Perrot A. (2021) Combined and synergic effect of algerian natural fibres and biopolymers on the reinforcement of extruded raw earth. *Construction and Building Materials*, **289**, 123211. https://doi.org/10.1016/j.conbuildmat.2021.123211

Bories C., Borredon M.-E., Verdrenne E. & Vilarem G. (2014) Development of eco-friendly porous fired clay bricks using pore-forming agents: A review. *Journal of Environmental Management*, **143**, 186–196. http://dx.doi.org/10.1016/j.jenvman.2014.05.006b

Bouguerra A., Diop M.B., Laurent J.P., Benmalek M.L. & Queneudec M. (1998) Effect ofmoisture content on the thermal effusivity of wood cement-based composites. *Journal of Physics D: Applied Physics*, **31**, 3457. DOI: 10.1088/0022-3727/31/24/008

Bourret J., Tessier-Doyen N., Guinebretiere R., Joussein E. & Smith D.S. (2015) Anisotropy of thermal conductivity and elastic properties of extruded clay-based materials: Evolution with thermal treatment. *Applied Clay Science*, 116–117, 150–157.

Bray J.B. & Curtis J.T. (1957) An ordination of the upland forest communities of Southern Wisconsin. *Ecological Monographs*, **27**, 326–349.

Buchner T., Kiefer T., Königsberger M., Jäger A. & Füssl J. (2021) Continuum micromechanics model for fired clay bricks: Upscaling of experimentally identified microstructuralfeaturesto macroscopic elastic stiffness and thermal conductivity. *Materials& Design*, **212**, 110212. https://doi.org/10.1016/j.matdes.2021.110212

Davis R.O.E. & Bennett H.H. (1927) *Grouping of Soils on the Basis of Mechanical Analysis*, Department circular 419, US Department of Agriculture, Washington, DC, USA, 15 pp.

De Lagarde J. (1983) *Initiation à l'Analyse des Données*. Dunod, Paris, 3rd edition, 157 pp.

Debnath N.K., Pabbisetty V.K., Sarkar K., Singh A., Majhi M.R. & Singh V.K. (2022) Preparation and characterization of semi-silica insulation refractory by utilizing lignite fly ash waste materials. *Construction and Building Materials*, **345**, 128321. https://doi.org/10.1016/j.conbuildmat.2022.128321

Dos Santos C.A., Librelotto L.I. & Jacintho C., (2014) Building with earth – Brazil's most popular raw earth building techniques and the opinion of experienced builders. *Key Engineering Materials*, **600**, 123–131.

Elavarasan S., Priya A.K., Raja Gurusamy R., Mohamed RiyasNaveeth J. & Natesh, S., (2021) Experimental study on compressed earth block using fly-ash stabilizer. *Materials Today: Proceedings*, **37**, 3597–3600. https://doi.org/10.1016/j.matpr.2020.09.641

Fabbri A., Morel J-C. & Gallipoli D. (2018) Assessing the performance of earth building materials: a review of recent developments. *RILEM Technical Letters*, **3**, 46–58.

Fadil-Djenabou S., Ndjigui P-D. & Mbey J.A. (2015) Mineralogical and physicochemical characterization of Ngaye alluvial clays (Northern Cameroon) and assessment of its suitability in ceramic production. *Journal of Asian Ceramic Societies*, **3**, 50–58, http://dx.doi.org/10.1016/j.jascer.2014.10.008

Gallipoli D., Bruno A.W., Perlot C. & Mendes J. (2017) A geotechnical perspective of raw earth building. *ActaGeotechnica*, **12**, 463–478.

Giada G., Caponetto R. & Nocera F. (2019) Hygrothermal Properties of Raw Earth Materials: A Literature Review. *Sustainability*, **11**, 5342. https://doi.org/10.3390/su11195342.

Gialanella S., Girardi F., Ischia G., Lonardelli I., Mattarelli M. & Montagna M. (2010) On the goethite to hematite phase transformation. *Journal of Thermal Analysis and Calorimetry*, **102**, 867–873.

Hadji F., Ihaddadene N., Ihaddadene R., Betga A., Charick A. & Logerais P.O. (2020) Thermal conductivity of two kinds of earthen building materials formerly used in Algeria. *Journal of Building Engineering*, **32**, 101823. https://doi.org/10.1016/j.jobe.2020.101823

He H., Yue Q., Su Y., Gao B., Gao Y., Wang J. & Yu H. (2012) Preparation and mechanism of the sintered bricks produced from Yellow River silt and red mud. *Journal of Hazardous Materials*, **203**, 53–61.

John E., Epping J.D. & Stephan D. (2019)The influence of the chemical and physical properties of C-S-H seeds on their potential to accelerate cement hydration. *Construction and Building Materials*, **228**, 116723. https://doi.org/10.1016/j.conbuildmat.2019.116723

Kaygusuz K. (2012) Energy for sustainable development: A case of developing countries. *Renewable and sustainable energy reviews*, **16**, 1116–1126.

Lee W.E., Souza G.P., McConville C.J., Tarvornpanich T. & Iqbal Y. (2008) Mullite formation in clays and clay-derived vitreous ceramics. *Journal of the European Ceramic Society*, **28**, 465–471.

Mansour M., Jelidi A., Cherif A. & Jabrallah S. (2016) Optimizing thermal and mechanical performance of compressed earth blocks (CEB). *Construction and Building Materials*, **104**, 44–51.

Meukam P., Jannot Y., Noumowe A. & Kofane T.C. (2004) Thermo physical characteristics of economical building materials. *Construction and Building Materials*, **18**,437–443.

Michot A., Smith D.S., Degot S. & Gault C. (2008) Thermal conductivity and specific heat of kaolinite: Evolution with thermal treatment. *Journal of the European Ceramic Society*, **28**, 2639–2644.

Murmu A.L. & Patel A. (2018) Towards sustainable bricks production: An overview. *Construction and Building Materials*, **165**, 112–125.

Ndjigui P-D, Mbey J.A., Fadil-Djenabou S., Onana V.L., Bayiga E.C., Enock Embom C. & Ekosse G-I. (2021) Characteristics of Kaolinitic Raw Materials from the Lokoundje River (Kribi, Cameroon) for Ceramic Applications. *Applied Sciences*, **11**, 6118. https://doi.org/10.3390/app11136118.

NjeumenNkayem D.E., Mbey J.A., Kenne Diffo B.B. & Njopwouo D. (2016) Preliminary study on the use of corn cob as pore forming agent in lightweight clay bricks: Physical and mechanical features. *Journal of Building Engineering*, **5**, 254-259. http://dx.doi.org/10.1016/j.jobe.2016.01.006

Nshimiyimana P., Fagel N., Messan A., Wetshondo D.O. & Courard L. (2020) Physico-chemical and mineralogical characterization of clay materials suitable for production of stabilized compressed earth blocks. *Construction and Building Materials*, **241**, 118097. https://doi.org/10.1016/j.conbuildmat.2020.118097

Okewale A.I. & Grobler H. (2022) Investigations into suitability of tropical clay for engineering applications. *Innovative Infrastructure Solutions*, **7**, 85. https://doi.org/10.1007/s41062-021-00683-x

Onana V.L., Ntouala R.F.D., Mbey J.A., Ngo'oZe A., Kabeyene V.K. & Ekodeck G.E. (2019) Mineralogy and preliminary assessment of the potential uses of alluvial clays from Batouri (Eastern-Cameroon). *Cerâmica*, **65**, 407–415. http://dx.doi.org/10.1590/0366-69132019653752626

Pountouenchi A., Njoya A., Mbey J.A., Mache J.R., Njoya D., Yongue F. R., Njopwouo D., Fagel N., Pilate P. & Van Parys L. (2023) Characterization of refractory bricks from selected Cameroonian kaolins. *Clay Minerals*, https://doi.org/10.1180/clm.2023.32

Reeves G.M., Sims I. & Cripps J.C., editors (2006) *Clay Materials Used in Construction*. Special Publications, 21, 513 pp., Geological Society of London, Engineering Geology.

Roudouane H.T., Mbey J.A., Bayiga E.C. & Ndjigui P.-D. (2020) Characterization and application tests of kaolinite clays from Aboudeia (southeastern Chad) in fired bricks making. *Scientific African*, **7**, e00294, https://doi.org/10.1016/j.sciaf.2020.e00294

Ruan H.D., Frost R.L. & Kloprogge J.T. (2001)The behavior of hydroxyl units of synthetic goethite and its dehydroxylated product hematite. *SpectrochimicaActa Part A: Molecular and Biomolecular Spectroscopy*, **57**, 2575–2586.

Ruan H.D., Frost R.L., Kloprogge J.T. & Duong L. (2002) Infrared spectroscopy of goethite dehydroxylation: III. FT-IR microscopy of in situ study of the thermal transformation of goethite to hematite. *SpectrochimicaActa Part A: Molecular and Biomolecular Spectroscopy*, **58**, 967–981.

Sore S.O., Messan A., Prud'homme E., Escadeillas G. & Tsobnang F. (2018) Stabilization of compressed earth blocks (CEBs) by geopolymer binder based on local materials from Burkina Faso. *Construction and Building Materials*, **165**, 333–345.

Souza G.P., Sanchez R. & De Hollanda J.N.F. (2002) Characteristics and physical-mechanical properties of fired kaolinitic materials. *Cerâmica*, **48**, 102–107.

Taallah B., Guettala A., Guettala S. & Kriker A. (2014) Mechanical properties and hygroscopicity behavior of compressed earth block filled by date palm fibers. *Construction and Building Materials*, **59**, 161–168.

Van Damme H. & Houben H. (2018) Earth concrete. Stabilization revisited. *Cement and Concrete Research*, **114**, 90–102.

Walker P. & Stace T. (1997) Properties of some cement stabilised compressed earth blocks and mortars. *Materials and Structures*, **30**, 545-551.

Wang G., Wang H. & Zhang N. (2017) *In situ* high temperature X-ray diffraction study of illite. *Applied Clay Science*, **146**, 254–263.

Ward J.H. (1963) Hierarchical grouping to optimize and objective function. *Journal of the American Statistical Association*, **58**, 236–44.

Yan Y.K. & Song Y.F. (2021) Research on application and thermal performance of raw earth material in building envelope. *Journal of Physics: Conference Series*, **1777**, 012041. DOI 10.1088/1742-6596/1777/1/012041.

Yoon Y.-G., Car R., Srolovitz D.J. & Scandolo S. (2004) Thermal conductivity of crystalline quartz from classical simulations. *Physical Review B*, **70**, 012302. https://link.aps.org/doi/10.1103/PhysRevB.70.012302

Yvon J., Lietard O. & Cases J.M. (1982) Minéralogie des argiles kaoliniques des Charentes. *Bulletin de Mineralogie*, **105**, 431–437.

Zhang L., Gustavsen A., Jelle B.P., Yang L., Gao T. & Wang Y. (2017) Thermal conductivity of cement stabilized earth blocks. *Construction and Building Materials*, **151**, 504–511.